Improvements in the Calibration of the NOAA-20 VIIRS Day-Night Band Low Gain Stage Using a Solar Diffuser

Junqiang Sun[1] and Xiaoxiong Xiong[2]

[1]Science Systems and Applications, Inc., 10210 Greenbelt Road, Suite 600, Lanham, MD 20706, USA
[2]Sciences and Exploration Directorate, NASA/GSFC, Greenbelt, MD 20771, USA

ABSTRACT

We aim to introduce and demonstrate several improvements that are applied to the on-orbit solar diffuser (SD) calibration of the day-night band (DNB) low gain stage (LGS) of the Visible Infrared Imaging Radiometer Suite (VIIRS) onboard the NOAA-20 satellite. The most important improvement is the expansion of the angular range, referred to "sweet spot", from 4° to 7.8° in order to increase the number of fully-illuminated scans considered for the SD calculation. The increase in scan number enables the completion of on-orbit calibration using the SD within one orbit, compared with the multiple orbits approach, which is required in the current standard approach applied in operational DNB LGS calibration coefficients look-up tables (LUTs) updates. The NOAA-20 DNB LGS calibration coefficients have been derived with the new methodology and the results show a more stable, smoother, and less noisy trend when compared with the current standard approach. The results also demonstrate that the NOAA-20 VIIRS DNB overall on-orbit performance has been very stable.

Keywords: NOAA-20, VIIRS, DNB, Low Gain Stage, Calibration, Improvements

1. Introduction

The second Visible Infrared Imaging Radiometer Suite (VIIRS) instrument is operated onboard the NOAA-20 satellite launched on 18 November 2017 [1,2]. The instrument is the first to follow the original VIIRS, which is housed in the Suomi National Polar-orbiting Partnership (SNPP) satellite that was launched on 28 October 2011 [3,4]. NOAA-20 VIIRS is a very similar instrument to the SNPP VIIRS, comprising of 14 reflective solar bands (RSBs) [5-7], 7 thermal emissive bands [8], and a day-night band (DNB) [9-11]. The DNB is a panchromatic band ranging from 0.5 μm to 0.9 μm designed for night scene observations [12]. The band covers a wide dynamic range, spanning over seven orders of magnitude, through operation in three gain settings – the low gain stage (LGS), the medium gain stage (MGS), and the high gain stage (HGS) [12,13].

The DNB LGS can be calibrated with the built-in solar diffuser (SD) panel using an approach similar to the RSB calibration [14], which uses the SD-measured data from the "sweet spot" [15,16]. When in the "sweet spot" range, the SD is fully illuminated by the sunlight, and the sunlight reflected from the SD can be accurately calculated [5,14-19]. The MGS and the HGS cannot be calibrated by utilizing the SD data during the same time period because they saturate during the calibration event. However, these stages can be calibrated via a ratio-based approach [20]. In this paper, we focus on the DNB LGS calibration using the onboard SD.

In the current SNPP and NOAA-20 VIIRS methodology, the "sweet spot" range for routine DNB LGS SD calibrations is exactly the same as that used in the RSB calibration, covering about 38 scans [15,16]. Due to the large number of aggregation modes (AMs) for data acquisition for the DNB, the number of scans within the "sweet spot" cannot meet the required number per complete calibration in just one orbit. This standard "sweet spot" is adequate to provide for a complete calibration of the RSBs in one orbit, but falls short for the DNB. The current operational strategy for the DNB calibration is to gather data from the "sweet spot" over multiple orbits, the number of which varies between 14 and 15, in one day to generate a set of complete DNB LGS calibration coefficients from the SD calibration [15,16]. This methodology not only complicates the calibration algorithm, but also does not guarantee the production of a complete set of calibration coefficients for the DNB for all the AMs from multiple orbits in the same day due to random coverage of the AMs in each orbit.

Recently, an improved methodology, referred to as "optimized calibration methodology", for the VIIRS DNB LGS SD calibration was developed and applied to SNPP VIIRS [21]. The key improvement in this methodology is to use a larger "sweet spot" such that a complete DNB LGS SD calibration can be implemented in one orbit. This requires the SD data in 72 continuous scans. It is noteworthy to emphasize that the SD must be fully illuminated by the sunlight for these 72 scans. It was demonstrated that there are just over 72 fully-illuminated scans during the time period before the instrument passes the Earth terminator at the south pole from night side to day side in each orbit [21]. The new methodology not only enables a complete set of DNB calibration coefficients, but also allows for higher accuracy and quality in the derivation of these coefficients [21]. In this analysis, the methodology is applied to the NOAA-20 VIIRS DNB LGS SD calibration. It is also demonstrated that the optimal calibration methodology works well for the NOAA-20 DNB, and that the derived calibration coefficients are indeed improved when compared to those derived with the standard method used currently in routine NOAA-20 VIIRS DNB LGS SD calibrations.

Section 2 provides some basic information about the VIIRS DNB. Section 3 describes the optimal calibration methodology for the DNB LGS SD calibration. Section 4 presents the improved results in the DNB F-factors and a brief discussion. Section 5 summarizes and concludes the findings of this manuscript.

2. Detectors, Aggregation Modes, and Data

2.1. Detectors and Gain Stages

The VIIRS DNB is composed of four charge-coupled device (CCD) detector arrays (two are for HGS, one for MGS, and one for LGS) [12]. This analysis focuses on the LGS. There are 672 subpixel detectors along-track and only 1 subpixel detector along-scan for the LGS. The 672 subpixel detectors along-track are aggregated on-board to create 16 pixels, "aggregated detectors", with a size of near-constant 742 meters along-track [12]. Hereafter, the "aggregated detectors" will simply be called "detectors".

2.2. Aggregation Modes

In order to achieve similar spatial size for each pixel during Earth observations, the DNB Earth view (EV) is divided into multiple aggregation zones (AZs) that are then grouped into pairs. Each pair of the aggregation zones has a corresponding AM [7]. The sampling time intervals for different AMs are different, and thus require separate calibration. Moreover, separate calibration is also needed for each of the 16 aggregated detectors, and for each of the two sides of the half-angle mirror (HAM) [11]. For SNPP VIIRS,

there are 64 AZs grouped into 32 pairs in the DNB EV [12]. The two zones in each pair are mirrored with respect to nadir as demonstrated in Fig. 1. For NOAA-20 VIIRS, there are 43 AZs corresponding to 21 pairs plus one AZ with AM 32 with no partner [10]. Unlike the SNPP VIIRS DNB, the NOAA-20 VIIRS DNB pairs are not mirrored with respect to the nadir but with the sample that is shifted towards the beginning of the scan from the nadir direction (Fig. 1) [10]. Altogether, the 32 and 22 AZs applied in the SNPP and NOAA-20 VIIRS DNB EV comprise a total of 1024 and 704 calibration coefficients for the SNPP and NOAA-20 VIIRS DNB LGS, respectively.

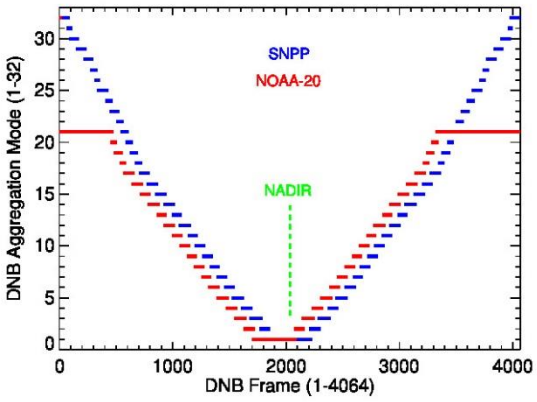

Fig. 1. VIIRS DNB EV AZs.

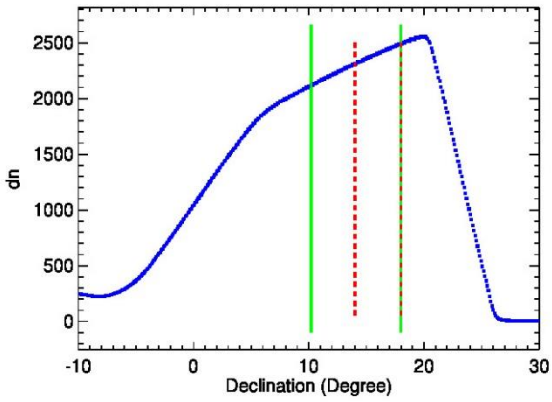

Fig. 2. NOAA-20 VIIRS band M6 detector 1 background-subtracted SD view response. Red dashed vertical lines: "sweet spot" used in current approach. Green solid lines: extended "sweet spot"

2.3. SD View Data

The VIIRS SD, made of specially-manufactured Spectralon with near-Lambertian reflectance properties, is installed inside of the VIIRS instrument primarily to serve as an on-orbit calibrator for the RSBs and the DNB [14]. This calibration can take place only during a short period in each orbit when the satellite crosses the Earth terminator at the south pole from the nightside to the dayside and the SD is fully illuminated [14,20]. Fig. 2 shows the background-subtracted instrument response digital count, denoted as dn, for NOAA-20 VIIRS band M6 detector 1 as a function of solar declination angle in the instrument coordinate system for a time interval covering the full illumination of the SD. The solar declination angle, starting from the nightside at a positive angle, decreases with time at a rate of about 3.6° per minute and reaches zero when the instrument is at the terminator [14,21]. Full illumination occurs in the solar-angle range from 6° to 20°. In principle, any data from the RSB observation of the SD within the full-illumination range can be used to derive the RSB and DNB calibration coefficients or F-factors.

2.4. Sweet Spot for LGS

In the current NOAA-20 RSB and DNB SD calibration, only the data in the solar declination angle range from 14° to 18° ("sweet spot") are selected for the VIIRS RSB and DNB SD calibration. About 38 scans are available from this "sweet spot". These scans provide an adequate dataset for the derivation of a complete set of RSB F-factors, but are insufficient to derive a complete set of calibration coefficients for the DNB [21]. As seen in Fig. 2 and mentioned previously, the SD full-illumination range varies in the solar angle range from 6° to 20°, which is much larger than the aforementioned "sweet spot". Since there is no

a-priori need for the DNB to have the same "sweet spot" as the RSBs, we can select a larger "sweet spot" for the DNB SD calibration. This expanded range will have enough scans, so as to provide an appropriate dataset for a complete calibration of the DNB, with a complete derivation of the calibration coefficients for each AM, detector, HAM side [21].

In the VIIRS SD view sector, the AM is fixed for each scan. Fig. 3 shows the NOAA-20 VIIRS DNB detector 1 SD view response versus solar declination angle (each data point corresponds to one scan). There are obvious discontinuities in the response profile. By analyzing data points in the plot, it can be seen that there is a discontinuity every 72 scans. Within the 72 scans, 64 have meaningful values, while the other 8 scans, in the range of the discontinuity, have no substantive data, and thus are not observed in the plot. Fig. 4 shows the AM number versus solar declination angle. A 72-scan cycle is clearly seen in Fig. 4. Similar to Fig. 3, there are only 64 AM values, which vary from 1 to 21 and 32 in each cycle. The AMs of the other 8 scans are numbered from 33 to 36 and designed for testing purposes. Nevertheless, 72 scans are needed to cover all AMs and two HAM sides.

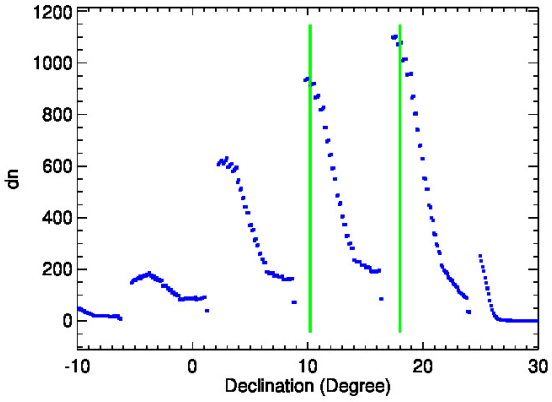

Fig. 3. NOAA-20 VIIRS DNB detector 1 SD view response.

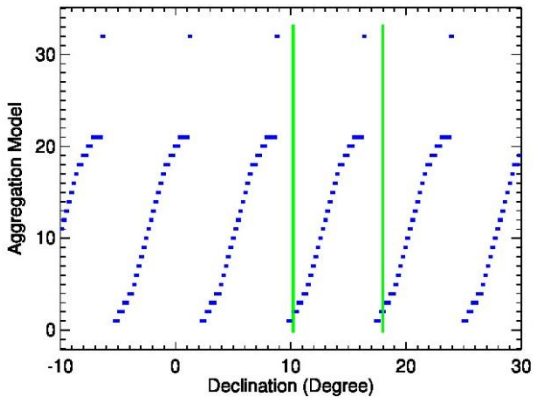

Fig. 4. NOAA-20 VIIRS DNB AM versus solar declination angle.

It is estimated and confirmed in the SNPP DNB LGS SD calibration that 72 scans span approximately 7.8° in declination angle [21]. As shown in Fig. 2, the full-illumination range during a SD calibration event spans over a range of about 14°, from 6° to 20°, which is larger than the required 7.8° range. This makes it possible to select a "sweet spot" within this range for the DNB calibration, which will cover all AMs and two HAM sides. Similar to the SNPP VIIRS DNB, the declination angle range can be selected from 10.2° to 18° as the "sweet spot" for the NOAA-20 VIIRS DNB. Occasionally, with this expanded "sweet spot" there will be a few more scans than the 72 needed, and for such cases the 72 scans with the largest declination angles within the "sweet spot" are selected for the DNB LGS SD calibration. The green vertical solid lines in Figs. 2-4 define the expanded "sweet spot" for the DNB, and the red vertical dashed lines Fig. 2 define the "sweet spot" currently used in the NOAA-20 RSB and DNB SD calibration for comparison.

As mentioned previously, AMs 1-21 are applied to the NOAA-20 VIIRS DNB EV retrievals. From Fig. 4, it can be seen that the SD view covers AMs 1-21 and 32, and thus the calibration coefficients can be derived for all needed AMs from the SD calibration. There are 64 effective scans, while there only 22 AMs and 2 HAM sides. Thus, there are some AMs that may have multiple scans for a given HAM side. This is different from the SNPP DNB, for which 32 AMs are applied in its EV, and only one scan corresponds to each given pair of AM and HAM side in the "sweet spot". In fact, there are four scans for each HAM side

of AM 21, two scans for each HAM side of AMs 1-4 and 18-20, and one scan for each HAM side for the rest of the AMs.

3. SD Calibration Algorithms

3.1. Radiance

For the VIIRS DNB, a linear approximation is applied to establish the relationship between the at-aperture radiance L and the background-subtracted instrument response dn,

$$L_{DNB}(Sample, Scan, D) = \frac{F_G(D,M,A)dn_{DNB,G}(Sample,Scan,D)}{RVS_{DNB}(\vartheta,M)}, \quad (1)$$

where *A* is the number of the AM, *Sample* is the pixel number along the scan direction, *Scan* is the scan number along the track direction, *D* is the detector number of the gain stage *G*, L_{DNB}*(Sample, Scan, D)* is the radiance at the sample of the scan observed by the detector *D*, *M* is the side number of the instrument HAM at the scan, and *G* is the gain stage of the detector *D* at the sample of the scan. $RVS_{DNB}(\vartheta,M)$ is the response-versus-scan (RVS)-angle of the DNB at the angle of incidence (AOI), ϑ, of the HAM *M*, which is a function of the sample and measured prelaunch. $F_G(D,M,A)$ is the calibration coefficient, known as the F-factor, for detector *D* of the gain stage *G*, HAM side *M* with aggregation mode *A*, which is inversely proportional to the on-orbit gain, and $dn_{DNB,G}(Sample,Scan,D)$ is the background-subtracted instrument response of detector *D* of gain stage *G* [21]. Equation (1) is applied to calculate the DNB EV radiance, where the DNB gain stage, *G*, is automatically selected for each pixel depending on the radiance level, but can be used for other view sectors as well. It can also be used to calculate the calibration coefficients if the incident radiance is known.

3.2. LGS Calibration Algorithms

As shown in Fig. 3, the DNB LGS does not saturate when its detectors view the SD in the full-illumination range. Thus the DNB can be calibrated by the SD similarly to the RSB calibration. The scattered sunlight radiance from the SD to the DNB can be expressed as,

$$L_{DNB,SD} = \frac{\tau_{SDS}cos(\theta_{SD})}{4\pi d_{ES}^2}\int L_{Sun}(\lambda)BRF_{SD,RTA}(\lambda)RSR_{DNB}(\lambda)d\lambda, \quad (2)$$

in the fully-illuminated range, where τ_{SDS} is the VF of the SD screen (SDS) placed in the front of the SD port, d_{ES} is the Earth-Sun distance in Astronomical Units (AU), θ_{SD} is the solar-zenith angle to the SD, $L_{Sun}(\lambda)$ is the solar radiance at the Earth-Sun distance of one AU, $BRF_{SD,RTA}(\lambda)$ is the bidirectional reflectance factor (BRF) of the SD for the view direction from the rotating telescope assembly (RTA) to the SD at wavelength λ, and $RSR_{DNB}(\lambda)$ is the detector-averaged relative spectral response (RSR) of the DNB. The BRF, $BRF_{SD,RTA}(\lambda)$, was measured during prelaunch at selected wavelengths and refined on-orbit using the yaw measurements at the wavelengths of the RSBs. It also changes on-orbit with time, and the change is tracked by the on-board SD Stability Monitor (SDSM).

Combining Eqs. (1) and (2), the DNB LGS calibration coefficients, F-factors, can be calculated using SD observations,

$$F_{LGS}(D,M,A) = \frac{RVS_{DNB}(\vartheta_{SD},M)L_{DNB,SD}(Scan,D)}{dn_{DNB,LGS,SD}(A,D)}, \quad (3)$$

where ϑ_{SD} is the AOI of the HAM for the SD view and $dn_{DNB,LGS,SD}(A,D)$ is the background-subtracted instrument response of the DNB LGS detector D with AM A [21]. As mentioned previously, there are 16 samples in the SD sector for the LGS along-scan, and $dn_{DNB,LGS,SD}(A,D)$ is the average of the 16 samples. As discussed in Sec. 2, the "sweet spot" for the LGS SD calibration is in the range of 10.2° to 18°, which is an expanded "sweet spot" compared to that used in the RSB calibration as well as that used in the algorithm theoretical basis document (ATBD) and by other groups. With this expanded "sweet spot", a complete set of LGS F-factors can be derived from the SD measurements of each orbit. Additionally, the calibration uncertainty of the daily-averaged F-factors is significantly reduced, as demonstrated in next section.

4. Calibration Coefficients and Performance

Fig. 5 shows the F-factors derived from the SD observations on 2 October 2018 for DNB LGS Detector 1 HAM 1 AMs 1 and 14, which are normalized by the mean value of all calibration coefficients of the two AMs for that day. The green symbols, filled triangles for Mode 1 and diamonds for Mode 14, are the new results derived from the optimized methodology [21] described in Secs. 2 and 3. The important outcome to note is that the new methodology, as expected, generates an F-factor for every orbit to give a total of 14 F-factors for the day, as demonstrated by each of the two aggregation modes in the plot. The red symbols in Fig. 5, empty squares for Mode 1 and squares with crosses for Mode 14, are the results derived from the current operational methodology. There are only 4 and 10 red symbols, instead of 14, for F-factors for AMs 1 and 14, respectively. In other words, AMs 1 and 14 are not covered in 10 and 4 orbits, respectively, using the current operational approach. In principle, the F-factors within each mode should remain about the same over the course of a day, since significant change of the instrument performance is not expected during a day of normal operation. However, it can be seen that each set of F-factors fluctuates with some uncertainty, about 0.5% for AM 1 and 0.8% for AM 14, over the course of a day due to various calibration errors and instrument noises. Nevertheless, the comparison between the solid green lines and dashed red lines clearly demonstrates that the F-factors derived using the extended "sweet spot" are not noisier than those from the original, narrower "sweet spot". This is a direct justification for the extension of the "sweet spot" described in Section 2 for the NOAA-20 VIIRS DNB. The same condition has been demonstrated for the SNPP VIIRS in our previous work [21].

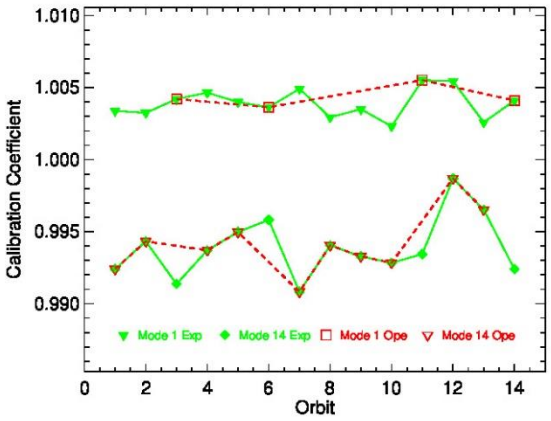

Fig. 5. NOAA-20 DNB detector 1 LGS calibration coefficients for AMs 1 and 14 derived from the SD calibration on October 2, 2018.

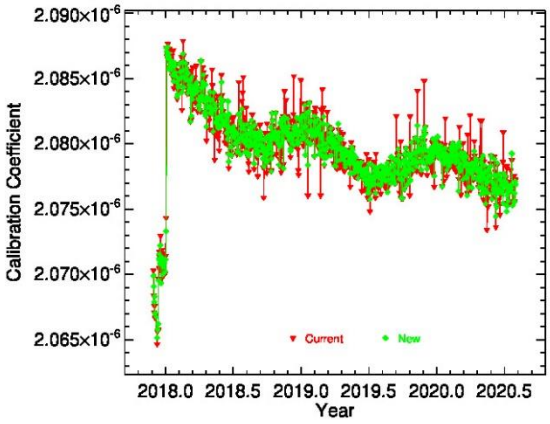

Fig. 6. Calibration coefficients for NOAA-20 VIIRS DNB AM 1 detector 1 HAM 1.

Fig. 6 shows the daily-averaged F-factors for DNB LGS Detector 1 AM 1 for the entire NOAA-20 VIIRS mission. The red triangles represent the F-factors derived using the current methodology with the original, narrow "sweet spot" and the green diamonds define those derived using the optimal calibration methodology with the extended "sweet spot". A fluctuation of about 0.4% in the F-factors presented by the green triangles is clearly seen in Fig. 6, while the fluctuation in those presented by the red diamonds is less than 0.15%, reduced by a factor 2.5. Thus, the calibration coefficients derived by using the new methodology have higher accuracy and quality, as well as resulting in a complete set of per-orbit coefficients. From Fig. 6, it is also clear that AM 1 is very stable, except for the 1% jump early in the NOAA-20 VIIRS mission. This spike occurred at the time when the NADIR door was opened. Afterwards, the gain of the AM only changes about 0.6% in the last two and half years. It is also worth mentioning that the gain, which is the inverse of the calibration coefficient, is increasing (as opposed to the expected decrease) with time. A small seasonal oscillation with an amplitude of 0.2% can be seen in the calibration coefficients as well, which might be induced by the errors in the SD BRF and the SD screen vignetting function (VF), the latter was measured during prelaunch and validated on-orbit using yaw measurements.

Fig. 7 shows the daily-averaged F-factors for DNB LGS HAM Side 1 Detector 1 AM 21 for the entire NOAA-20 VIIRS mission. Similar to Mode 1 (Fig. 6), the red triangles define the F-factors derived using the current operational methodology with the original, narrow "sweet spot" and the green diamonds represent those derived using the optimal calibration methodology with an extended "sweet spot". The results derived with the new methodology are less noisy than those derived using the current methodology. When compared to Fig. 6, it can also be seen that the calibration coefficients derived from the SD calibration for AM 21 are noisier than those from AM 1. The fluctuation in the coefficients of AM 21 derived with the new methodology is about 0.3%, twice as large as that from AM 1. The larger fluctuation in the F-factors of AM 21 is mainly due to the reduction of the collection time for each sample (smaller dn and smaller SNR).

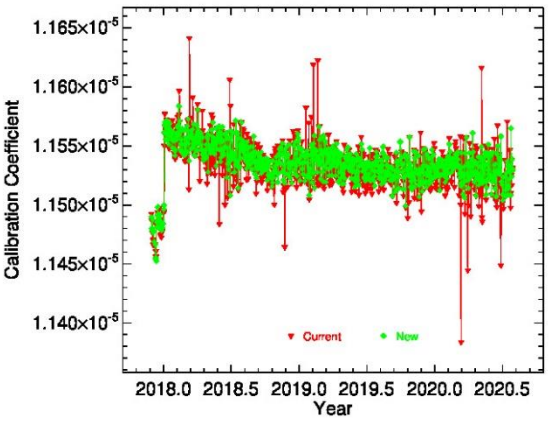

Fig. 7. Calibration coefficients for NOAA-20 VIIRS DNB AM 21 detector 1 HAM 1.

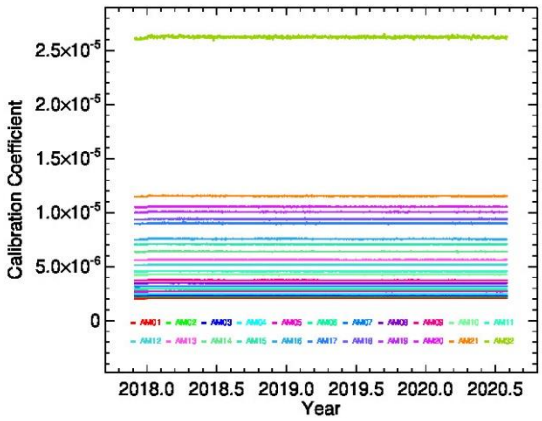

Fig. 8. Calibration coefficients for NOAA-20 VIIRS DNB AMs 1-21 and 32 detector 1 HAM 1.

Fig. 8 shows the daily-averaged F-factors, derived with the optimal methodology, of HAM side 1 detector 1 for all 22 AMs, AMs 1-21 and AM 32, applied to the EV for the entire mission. These all change smoothly with time, except for the jump of about 1% early in the NOAA-20 VIIRS mission. The F-factors are strongly aggregation-mode-dependent due to differences in data collection time [21]. AM 1 has the largest data collection time for each sample, and thus the largest gain, resulting in the smallest F-factor for

a given calibration event. Since the gain and F-factor are inversely proportional to each other, and data collection times decrease with AM number to give smaller gains, the F-factors then increase with AM number (Fig. 8). Fig. 9 shows the F-factors normalized to the first measurement for HAM side 1 detector 1 for all AMs. It is seen in Fig. 9 that the F-factors for all AMs perform consistently, all jumping about 1% early in the instrument's mission and then decreasing with time at about the same rate for any given time. This is expected, since the main differences amongst the modes are those in data collection times. It is also evident from Fig. 9 that the fluctuations in the calibration coefficients become larger with AM number. This is understandable, since the data collection time decreases with the AM number.

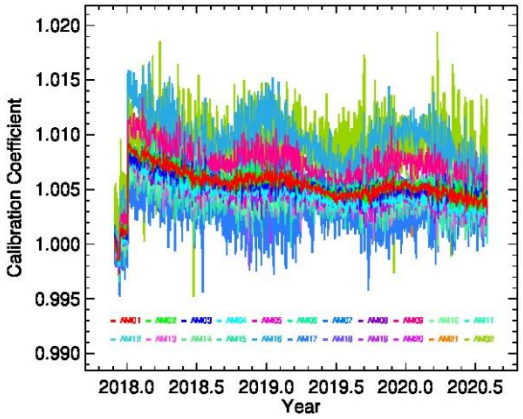

Fig. 9. Calibration coefficients for NOAA-20 VIIRS DNB all AMs, AMs 1-21 and AM 32, detector 1 HAM 1. The calibration coefficients for each AM are normalized to its first measurement.

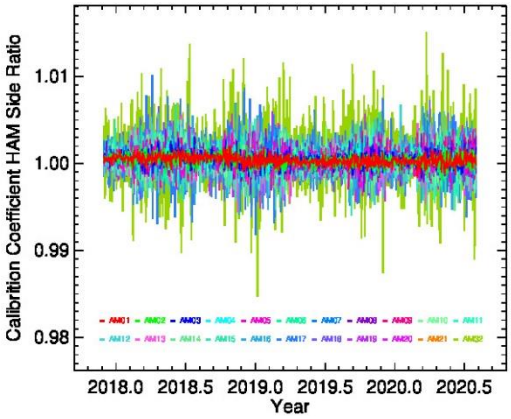

Fig. 10. Calibration coefficients HAM side rations for NOAA-20 VIIRS DNB all AMs, AMs 1-21 and AM 32, detector 1.

Lastly, Fig. 10 shows the HAM side ratios for the calibration coefficients for all AMs. The ratios for AM 1 are quite stable. Hence, there is no long-term trend observed, and the fluctuation of the ratios is less than 0.2% for AM 1 and increases with AM number. Moreover, there are no long-term trends observed in the ratios of all other AMs, even though these become larger with the increase of the AM number. In short, the two HAM sides change with time at about the same rate.

5. Summary

The optimal calibration methodology of the VIIRS DNB LGS SD calibration has been applied to NOAA-20 VIIRS DNB LGS SD calibration. The methodology enables a complete DNB calibration within one orbit. The NOAA-20 VIIRS DNB LGS calibration coefficients are derived from the SD observations for the entire instrument's mission. The derived coefficients smoothly change with time at slow rates, which are about the same for all AMs, HAM sides, and detectors; indicating that the NOAA-20 VIIRS DNB is performing well. The actual values of the calibration coefficients increase with AM number, and the fluctuations of these calibration coefficients increase with AM number as well. This phenomenon is due to the fact that the data collection time for each sample decreases with the AM number. It is also demonstrated that the fluctuations in the calibration coefficients derived the optimal methodology are much smaller than those in the calibration coefficients derived with the current operational methodology - indicating that the optimal calibration methodology significantly improves the calibration results over the current approach. The overall results clearly demonstrate the success and superiority of the optimal calibration methodology for the aspects presented. The optimal calibration methodology has been successfully applied to SNPP and

NOAA-20 VIIRS, and its advantages over the current operational method is showcased. The optimal methodology can be directly applied to future VIIRS instruments.

Acknowledgements

We would like to thank Carlos Perez and Gal Sarid for their valuable comments and suggestions. The views, opinions, and findings contained in this paper are those of the authors and should not be construed as an official NASA or U.S. Government position, policy, or decision.

References

1. C. Cao, S. Blonski, W. Wang, S. Uprety, X. Shao, J. Choi, E. Lynch, and S. Kalluri, "NOAA-20 VIIRS on-orbit performance, data quality, and operational Cal/Val support", Proc. SPIE 10781, 107810K (2018).
2. X. Xiong, H. Oudrari, J. McIntire, N. Lei, K. Chiang, and A. Angal, "Initial calibration activities and performance assessments of NOAA-20 VIIRS", Proc. SPIE 10781, 107810L (2018).
3. C. Cao, F. Deluccia, X. Xiong, R. Wolfe, and F. Weng, "Early on-orbit performance of the Visible Infrared Imaging Radiometer Suite (VIIRS) onboard the Suomi National Polar-orbiting Partnership (S-NPP) satellite," IEEE Trans. Geosci. Remote Sens., 52, 1142–1156, 2014.
4. X. Xiong, J. Butler, K. Chiang, B. Efremova, J. Fulbright, N. Lei, J. McIntire, H. Oudrari, J. Sun, Z. Wang, and A. Wu, "VIIRS on-orbit calibration methodology and performance," J. Geophys. Res. Atmos., 119, 5065–5078, 2014.
5. Sun, J., M. Chu, and M. Wang, "On-orbit characterization of the VIIRS solar diffuser and attenuation screens for NOAA-20 using yaw measurements", Appl. Opt., 57, 6605-6619 (2018).
6. N. Lei, K. Twedt, X. Chen, and X. Xiong, "Initial radiometric calibration status and performance of NOAA-20 VIIRS reflective solar bands", Proc. SPIE 10781, 107810M (2018).
7. J. Sun and X. Xiong, "NOAA-20 VIIRS reflective solar bands onorbit calibration," Proc. SPIE 1115, 111511J (2019).
8. Y. Li, X. Xiong, J. McIntire, A. Angal, S. Gusev, and K. Chiang. "NOAA-20 VIIRS thermal emissive bands on-orbit performance", Proc. SPIE 10781, 107810N (2018).
9. 4. J. Sun and M. Wang, "Optimized calibration methodology of VIIRS day-night band low-gain stage using a solar diffuser", Appl. Opt., 56, 4433-4442 (2017).
10. W. Wang, and C. Cao, "NOAA-20 VIIRS DNB Aggregation Mode Change: Prelaunch Efforts and on-Orbit Verification/Validation Results. IEEE Journal of Selected Topics in Applied Earth Observations and Remote Sensing", 12, 2015-2023 (2019).
11. H. Chen, X. Xiong, D. O. Link, C. Sun, and K. Chiang, "NOAA-20 Visible Infrared Imaging Radiometer Suite day–night band on-orbit calibration and performance", Journal of Applied Remote Sensing, in press.
12. S. Mills, "VIIRS Radiometric Calibration Algorithm Theoretical Basis Document", Doc. No.: D43777, Northrop Grumman Aerospace Systems: Redondo Beach, CA, USA, 2010.
13. S. D. Miller, S. P. Mills, C. D. Elvidge, D. T. Lindsey, T. F. Lee, J. D. Hawkins, "Suomi satellite brings to light a unique frontier of nighttime environmental sensing capabilities", Proc. Nat. Acad. Sci., 109, 15707–15710, 2012.
14. J. Sun and M. Wang, "On-orbit calibration of Visible Infrared Imaging Radiometer Suite reflective solar bands and its challenges using a solar diffuser ", Appl Opt., 7210-7223, 2015.

15. J. Geis, C. Florio, D. Moyer, K. Rausch, F. J. De Luccia, “VIIRS Day-Night Band Gain and Offset Determination and Performance”, Proc. SPIE, 8510, 851012, 2012.
16. L. B. Liao, S. Weiss, S. Mills, B. Hauss, “Suomi NPP VIIRS day-night band on-orbit performance”, J. Geophys. Res. Atmos., 118, 12707–12718, 2013.
17. H. Chen, X.Xiong, C. Sun, X. Chen and K. Chiang, “Suomi-NPP VIIRS day-night band on-orbit calibration and performance”, Journal of applied remote sensing, Vol. 11(3), 036019 (2017).
18. C. Sun, T. Schwarting, K. Chiang, H. Chen, Se. Gusev, and X. Xiong, “Reprocessing of S-NPP VIIRS DNB detector gains and dark offsets”, Proc. SPIE 11127, 111271U (2019).
19. T. Wilson and X. Xiong, "Intercomparison of the SNPP and NOAA-20 VIIRS DNB High-Gain Stage Using Observations of Bright Stars," in IEEE Transactions on Geoscience and Remote Sensing, doi: 10.1109/TGRS.2020.2986094.
20. S. Lee, J. McIntire, H. Oudrari, T. Schwarting, X. Xiong, “A new method for Suomi-NPP VIIRS day-night band on-orbit radiometric calibration”, IEEE Trans. Geosci. Remote Sens., 53, 324–334, 2015.
21. J. Sun and M. Wang, "Optimized calibration methodology of VIIRS day-night band low-gain stage using a solar diffuser", Appl. Opt., 56, 4433-4442 (2017).